Benchmark Study of PHITS for High-Energy Neutron Spectrum Using Activation Foil Method at NDPS

Jinhong Kim[1], Sinchul Kang[2], Kyoungho Tshoo[2], Jaesung Kim[1,2], Danhye Gil[2], Young-Ouk Lee[2], Cheolmin Ham [2*], Hyungjin Shim [1*]
[1]*Department of Nuclear Engineering, Seoul National University, Seoul 08826*
[2]*Institute for Rare Isotope Science, Institute for Basic Science, Daejeon 34000*
[*]*Corresponding author:cmham@ibs.re.kr, shimhj@snu.ac.kr*

***Keywords :** Activation foil, PHITS, Heavy-ion beam, NDPS, RAON

1. Introduction

The activation foil method is one of the most effective techniques for characterizing neutron energy and angular spectra in harsh environments, such as nuclear reactor cores with high temperature and pressure. Furthermore, it serves as an alternative method for neutron spectrum analysis in facilities where the Time-of-Flight (ToF) technique is not applicable. Despite these advantages, experimental neutron cross-section data for energies exceeding 20 MeV remain limited.

Nuclear Data Production System (NDPS) is a neutron experimental system at the Rare Isotope Accelerator complex for ON-line experiments (RAON) heavy ion accelerator that produces neutrons with energies of several tens of MeV by bombarding a graphite target with ^{40}Ar ions. In this study, an activation foil experiment was conducted at NDPS. The experimentally measured end-of-beam (EOB) activities of the detector foils were compared with the results simulated using the Particle and Heavy Ion Transport code System (PHITS) to validate the experimental methodology and the reliability of the high-energy cross-section data.

2. Methods and Results

In this section, two distinct methods employed to determine the EOB activities (A_0) of the detector foils and their corresponding results are described. First, an experimental approach was conducted by irradiating a natural carbon target with an 18.4 MeV/u ^{40}Ar heavy-ion beam at the RAON heavy ion accelerator facility [3]. The produced neutron interacted with the activation foils, and the emitted gamma rays were measured using a High-Purity Germanium (HPGe) detector to determine A_0 values for objective reactions (see TABLE I).

TABLE I: Threshold energy and half-life of each objective reaction

Foil	Objective Reaction	Half-life	Threshold [MeV]
^{27}Al	^{27}Al (n,x) ^{24}Na	14.96 h	3.6
^{197}Au	^{197}Au (n,2n) ^{196}Au	9.61 h	8.1
^{209}Bi	^{209}Bi (n,4n) ^{206}Bi	6.24 d	22.6
	^{209}Bi (n,5n) ^{205}Bi	14.91 d	29.6
	^{209}Bi (n,6n) ^{204}Bi	11.28 h	38.2

Second, a computational method was utilized where the neutron flux was derived using PHITS simulations. This neutron flux was integrated with the neutron-induced reaction cross sections responsible for the activation of the detector foils, from which the A_0 values were calculated.

2.1 Experimental methodology

The irradiation was carried out using a neutron beam at the RAON facility. A 18.4 MeV/u ^{40}Ar ion beam bombarded a 29 mm-thick natural carbon target inside a vacuum chamber to produce neutrons. Several activation foils were irradiated for 7,560 s under a constant ion beam current of 70 pnA to generate sufficient induced activity for subsequent gamma-ray measurements of the reaction products.

To maximize the incident neutron fluence, the detector assembly positioned on the beam axis. The assembly consisted of a stacked configuration of multiple detector foils (including ^{27}Al, ^{197}Au, and ^{209}Bi) to exploit their distinct energy threshold characteristics for neutron interaction.

Each foil, with dimensions of 10 × 10 × 1 mm^3 (except for the Au foil, which was 0.1 mm thick), was arranged in a sequence along the beam path at a distance of 10 cm from the target. This stacked arrangement allowed for the simultaneous measurement of various reactions within the same neutron field, facilitating a comprehensive comparison of energy-dependent yields. The layout of the target and foil assembly is illustrated in Fig. 1.

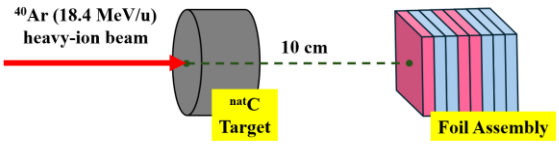

Fig. 1. Schematic diagram of the natural carbon target and activation foil assembly

Following the irradiation, the activities of the foils were quantified using a HPGe detector [1]. For the ^{209}Bi foil, in particular, two separate counting sessions were conducted to accommodate the significantly different half-lives of its reaction products. This strategic

separation of detection times allowed for the optimal observation of each objective radionuclide, ensuring sufficient statistical precision across all measured energy thresholds.

The EOB activities were derived from the HPGe measurement results using Eq.(1). For each reaction product, the activities obtained from multiple gamma-ray peaks were averaged by applying weights based on their respective statistical uncertainties. The resulting average values, along with their associated errors, are summarized in TABLE II.

$$A_0 = \frac{\lambda C}{\epsilon I_\gamma \, e^{\lambda t_0}(e^{-\lambda t_1} - e^{-\lambda t_2})} \qquad (1)$$

In Eq.(1), C, ϵ, and I_γ represent the net counts, overall counting efficiency, and gamma-ray intensity, respectively, while t_0, t_1, and t_2 denote the irradiation, start, and end times of the measurement.

TABLE II. Experimental end-of-beam activities for each activation reaction

Reaction	A_0 [Bq]	ΔA_0 [Bq]
^{27}Al (n,x) ^{24}Na	138.1333	3.7731
^{197}Au (n,2n) ^{196}Au	317.7826	1.8897
^{209}Bi (n,4n) ^{206}Bi	16.2678	0.1099
^{209}Bi (n,5n) ^{205}Bi	8.3714	0.2356
^{209}Bi (n,6n) ^{204}Bi	8.3035	0.2546

2.2 Calculational methodology

To determine the activities through computational methods, a multi-step computational approach was employed. First, the neutron flux was derived using the PHITS code [2] by modeling the experimental geometry. Then, the reaction rates were determined by combining the flux with nuclear cross-section data. Finally, the EOB activities were calculated by solving the governing differential equations that account for the beam-on period and the specific foil properties.

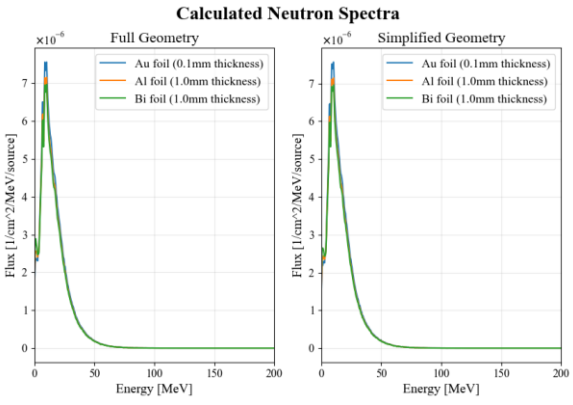

Fig. 2. Simulated neutron energy spectra by PHITS for the full and simplified geometry models (10^{10} primary histories).

The PHITS simulations were conducted under two distinct modeling scenarios to evaluate the influence of the environment on the result: a detailed model precisely replicating the actual experimental facility, and a simplified model consisting only of the target and foil assembly. From these simulations, the energy-dependent neutron flux within each foil was obtained for each configuration, as presented in Fig. 2

To ensure an accurate evaluation of reaction rates, it is essential to employ nuclear data libraries that provide reliable cross-section values in the high-energy region. In this study, the neutron reaction cross-sections for each objective reaction were retrieved from the TENDL-2009 [4] and IRDFF-II [5] libraries, which offer comprehensive data for energies up to 200 MeV (see Fig. 3).

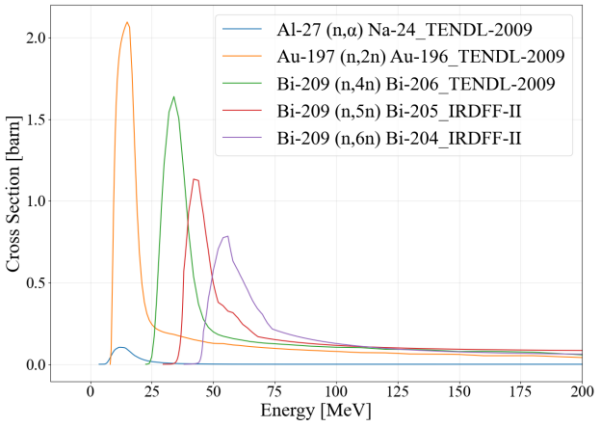

Fig. 3. Neutron reaction cross-sections for objective reactions retrieved from TENDL-2009 and IRDFF-II libraries up to 200 MeV.

The reaction rate R was subsequently determined using the following integration:

$$R = N \int_{E_{min}}^{E_{max}} \sigma(E)\phi(E)dE \qquad (2)$$

where N is the number of target nuclei in the detector foil. $\sigma(E)$ and $\phi(E)$ represent the energy-dependent neutron reaction cross-section and the calculated neutron flux.

To calculate the end-of-beam activity, a differential equation accounting for the production and decay of radionuclides during irradiation was established:

$$\frac{dN(t)}{dt} = R \cdot I(t) - \lambda N(t) \qquad (3)$$

where λ is the decay constant of the product isotope for objective reaction and $I(t)$ is the particle beam current signal deduced from actual beam current signal from ACCT sensor. By solving Eq. (2) the calculated A_0 values were derived for comparison with experimental results.

The results demonstrate that the level of detail in the environmental modeling has a negligible impact on the calculated activities, indicating that the neutron field is primarily governed by the immediate surrounding

materials (see TABLE III). And the uncertainties are attributed to the statistical errors of the Monte Carlo method in the PHITS simulations and the uncertainties in the number of target nuclides within the foils.

TABLE III. Calculated end-of-beam activities for full geometry and simplified geometry situations.

Reaction	Full geo. $(A_0 \pm \Delta A_0)$ [Bq]	Simplfied geo. $(A_0 \pm \Delta A_0)$ [Bq]
^{27}Al (n,x) ^{24}Na	41.290 ± 0.049	41.250 ± 0.049
^{197}Au (n,2n) ^{196}Au	118.80 ± 0.15	118.67 ± 0.15
^{209}Bi (n,4n) ^{206}Bi	12.879 ± 0.034	12.907 ± 0.038
^{209}Bi (n,5n) ^{205}Bi	1.4370 ± 0.006	1.4415 ± 0.006
^{209}Bi (n,6n) ^{204}Bi	13.379 ± 0.084	13.426 ± 0.085

2.3 Comparison of results

The calculation-to-experiment (C/E) ratios for each objective reaction are summarized in TABLE IV and visualized in Fig. 4. A primary observation from the data is the general tendency of the PHITS simulation to underestimate the experimental activation yields. For the majority of the reactions the C/E ratios fall well below unity, ranging from approximately 0.17 to 0.79. The most pronounced underestimation occurs in the ^{209}Bi (n,5n) ^{205}Bi reaction, which yields a C/E ratio of roughly 0.17.

Conversely, a distinct overestimation is observed in the ^{209}Bi (n,6n) ^{204}Bi reaction, which possesses the highest threshold energy among the analyzed channels. The calculated activity for this reaction is approximately 1.6 times higher than the experimental value.

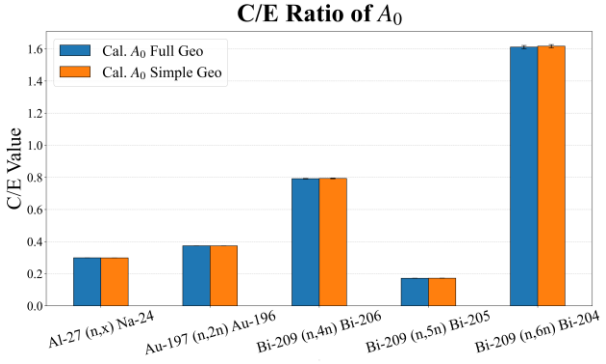

Fig. 4. Comparison of calculated and experimental end-of-beam activities (A_0) for various activation reactions, expressed as C/E ratios. Error bars represent statistical uncertainties (mostly < 1%), which are barely visible; exact values are listed in TABLE IV.

TABLE IV. Comparison of calculation-to-experiment (C/E) ratios for different geometry modeling scenarios

Reaction	C/E (full geo.)	C/E (Sim. geo.)
^{27}Al (n,x) ^{24}Na	0.299 ± 0.008	0.297 ± 0.008
^{197}Au (n,2n) ^{196}Au	0.374 ± 0.002	0.373 ± 0.002
^{209}Bi (n,4n) ^{206}Bi	0.792 ± 0.011	0.793 ± 0.011
^{209}Bi (n,5n) ^{205}Bi	0.172 ± 0.015	0.172 ± 0.015
^{209}Bi (n,6n) ^{204}Bi	1.611 ± 0.050	1.617 ± 0.050

3. Conclusions

In this study, the neutron produced by an 18.4 MeV/u ^{40}Ar heavy-ion beam on a natural carbon target was characterized using the activation foil method at NDPS. The experimental EOB activities were compared with PHITS simulations to evaluate the predictive accuracy of the code in high-energy regions. The results indicated that there was no significant difference between the detailed (full) and simplified geometry models in the PHITS simulations. Excluding the ^{209}Bi (n,6n) ^{204}Bi reaction, which has the highest threshold energy, the C/E ratios ranged from 0.17 to 0.79, demonstrating that the calculated values generally underestimated the experimental results. Conversely, for the very high-threshold reaction, the code exhibited an overestimation, yielding a C/E ratio of approximately 1.6.

Since the geometric modeling detail had a negligible impact, it is plausible that these discrepancies are associated with the uncertainties in the nuclear data libraries for high-threshold reactions, as well as potential limitations in the physics models used in PHITS for predicting high-energy neutron spectra. Therefore, to further investigate the exact causes of these discrepancies, future work will focus on comparative analyses using various nuclear data libraries and different physics model options within the PHITS code.

ACKNOWLEDGEMENTS

We would like to thank the accelerator division researchers of RAON. This work was supported by the Institute for Basic Science (IBS-I001-D1) and by the National Research Foundation of Korea (NRF) funded by Ministry of Science and ICT (RS-2023-00282876).

REFERENCES

[1] G. F. Knoll, Radiation Detection and Measurement, John Wiley & Sons, New York, pp.767-770, 1999.
[2] T. Sato, Y. Iwamoto, and S. Hashimoto, Features of Particle and Heavy Ion Transport code System (PHITS) version 3.02, Journal of Nuclear Science and Technology, Vol. 55, No. 6, pp. 684-690, 2018.
[3] C. Ham et al., Overview of nuclear data production system at RAON, Nuclear Instruments and Methods in Physics Research B, Vol. 541, pp. 363-365, 2023.
[4] A. J. Koning and D. Rochman, Modern Nuclear Data Evaluation with the TALYS Code System, Nuclear Data Sheets, Vol. 113, No. 12, pp. 2841-2934, 2012.
[5] A. Trkov et al., IRDFF-II : A New Neutron Metrology Library, Nuclear Data Sheets, Vol. 163, pp. 1-108, 2020.